

Increasing the lifetime of confined electronic states in an artificial quantum structure

Marco Weiss¹, Michael Schelchshorn, Fabian Stilp¹, Alfred J. Weymouth¹, and Franz J. Giessibl^{1*}
Institute of Experimental and Applied Physics, University of Regensburg, 93053 Regensburg, Germany

 (Received 9 April 2024; accepted 21 May 2024; published 17 June 2024)

Understanding and tuning the factors influencing the lifetime of confined electronic states is a basic concept of quantum mechanics, whereas achieving large lifetimes in artificial nanostructures holds great potential for advancing quantum technologies. An example of such artificial structures are CO-based quantum corrals. In this study, tunneling spectroscopy measurements reveal a strong correlation between the size of the quantum corral and spectral width, characterized by a predominant Gaussian line shape. We attribute this dominant Gaussian-shaped lifetime broadening to the interaction of surface state electrons with the corral boundary. To further investigate this phenomenon, we constructed corrals of varying wall densities. Our findings indicate that elastic processes, such as tunneling, are more sensitive to the wall density than coupling to the bulk.

DOI: [10.1103/PhysRevB.109.235422](https://doi.org/10.1103/PhysRevB.109.235422)

I. INTRODUCTION

In a neutral atom, electronically excited states typically decay within a few nanoseconds [1]. The probability of the electron remaining in an excited state decreases exponentially with time, therefore observed spectral line shape of the decay is Lorentzian. For certain realizations of artificial atoms (e.g., quantum dots) [2], the observed spectral peaks are also well-described by Lorentzian functions (e.g., Refs. [3–5]). The spectral line shapes and their widths are a measure of not only the lifetimes of the confined states but also the lifetime limiting mechanisms within artificial atoms. Understanding these mechanisms is vital for designing quantum dots that carry confined electronic states with long lifetimes. Long-lived confined states have been proposed for applications in quantum sensing, quantum computing, and for creating artificial quantum simulators (e.g., Refs. [6–13]).

We investigate a realization of an artificial atom called a quantum corral, which we constructed by atomic manipulation of adsorbates on the surface of a noble metal using scanning probe microscopy [14]. A quantum corral confines the quasi-free 2D electron gas present on the surface [15], resulting in a set of resonant eigenstates. While the original corral, consisting of Fe adatoms arranged in a circle on Cu(111), has been published already in 1993 [14], quantum corrals have since been constructed on more exotic surfaces including semiconductors [6], a Rashba surface alloy [16], a proximity superconductor [17], and topological insulators [18]. Interpreting the spectral peaks of these corral states requires a thorough understanding of the lifetime limitations.

There are three mechanisms which influence the lifetime of surface state electrons: electron-phonon scattering, electron-electron scattering and electron-defect scattering [e.g. 19–30]. The common property of electron-phonon scattering and electron-electron scattering is a temporally constant and

spatially homogeneous scattering background for surface state electrons which results in an exponentially decreasing survival probability in the time domain, corresponding to a Lorentzian peak shape in the energy domain [29]. For studies of quantum corrals, electron-defect scattering corresponds to scattering at the corral walls. While randomly distributed defects should also result in a Lorentzian contribution to the line shape [29], the defects that make up the corral walls are not randomly spaced. Considering the corral walls as well-arranged defects, a dense wall not only limits the lateral transmission out of the corral but also increases scattering into bulk states.

Since the realization of the first quantum corral with Fe adatoms [14], the electron-wall interaction has been a topic of theoretical investigation. Using multiple scattering theory with an additional absorbing channel at δ -peak shaped scattering potentials, it was concluded that the widths of the corral states energy distributions (spectral peaks) are mainly dictated by the absorbing channel (e.g., scattering to bulk states). An estimate indicated that approximately 25% of an incident wave is transmitted and about 50% is absorbed [31]. Other studies also emphasize the significant role of scattering to bulk states in reproducing the energy width of corral states in simulations [32,33]. However, some theoretical considerations of quantum corrals are based entirely on elastic mechanisms. For instance, a model representing the adsorbates of the corral as finite-height cylindrical potentials concluded that bulk coupling is not necessary to reproduce the energetic behavior and standing wave pattern of the corral [34]. Other theoretical considerations with Gaussian-shaped potentials can also reproduce the energetic behavior of a quantum corral without additional lossy channels [35].

In this article we characterize the energy distributions of quantum corral states by means of spatially high resolved scanning tunneling spectroscopy (STS) measurements. By comparing two corrals of different sizes, we show that the spectral widths are fundamentally influenced by the confinement, i.e., the corral wall. Moreover, we find that the line

*franz.giessibl@ur.de

shape of the energy distributions is not Lorentzian as it was previously reported [14], but Gaussian. The energy dependence of the corresponding widths prompts us to propose a classical model which connects the lifetime of the corral states to the average path length of a confined surface state electron.

To further understand the influence of the interaction of the electrons with the corral wall, we constructed corrals with various densities of adsorbates in the walls. Corrals with a denser wall host states with narrower energy distributions, allowing us to conclude that transmission (i.e., tunneling through the corral wall) is more sensitive to the wall density than coupling to the bulk.

II. FOUNDATIONS OF A QUANTUM CORRAL

The first quantum corral, built with a scanning tunneling microscope (STM), was created by arranging 48 Fe adatoms in a circular shape on Cu(111) [14]. While this artificial structure showed discrete energy states, a detailed investigation with large voltage variation was difficult because the corral wall was not stable [14]. This can be attributed to the weak bonding of Fe on Cu(111) [36]. By using a more stable wall than the original quantum corral, we are able to investigate states far away from the Fermi level and to precisely measure their spectral widths and line shapes. Carbon monoxide (CO) binds six times stronger to Cu(111) than Fe [36,37], making it a good candidate for creating stable artificial structures. Spectroscopic STM measurements on CO-based structures therefore show the desired stability and allow for a larger voltage window [16,38–40] to perform a detailed analysis of the corral's energy levels.

The spatial behavior of states in a ring-shaped quantum corral is almost identical to the one of states in an infinitely high cylindrical potential well [14,41], commonly known as the hard-wall model. Solving the Schrödinger equation for the hard-wall model yields the solutions $\Psi_{n,l}(r, \phi, z) = \psi_{n,l}(r) \times \psi_l(\phi) \times \psi(z)$, where n is the main quantum number and l the angular momentum quantum number. The radial distance from the center of the corral is denoted by r , ϕ is the azimuthal angle and z is the direction perpendicular to the surface. Here, $\psi_{n,l}(r)$ describes the radial-dependent component of the wave function including Bessel functions of the first kind, while $\psi_l(\phi) = 1/\sqrt{2\pi} \times \exp(il\phi)$ describes the angular dependence. The z component of the Shockley surface state remains unaffected by the cylindrical potential well. Above the surface ($z > 0$), $\psi(z) \propto \exp(-\kappa z)$ with the decay constant κ [41]. The absolute square of each wave function, which can be measured with STM, gives the probability density $|\Psi_{n,l}(r, \phi, z_0)|^2 = |\psi_{n,l}(r)|^2 \times |\psi_l(\phi)|^2 \times |\psi(z_0)|^2 = |\psi_{n,l}(r)|^2 \times 1/2\pi \times C_{z_0}$. As measurements for each corral were performed at the same tip-sample distance, z_0 , and κ is the same for every corral state [41], the z component $|\psi(z_0)|^2$ can be expressed as a factor C_{z_0} that only depends on z_0 . For a more detailed discussion and calculations see the Supplemental Material of Stilp *et al.* [41]. In this work corral states are characterized by their main quantum number n and their angular momentum quantum number l .

For the initial line shape analysis, measurements (see SM1 of the Supplemental Material [42] for experimental details) were taken of two differently sized CO corrals: one with a

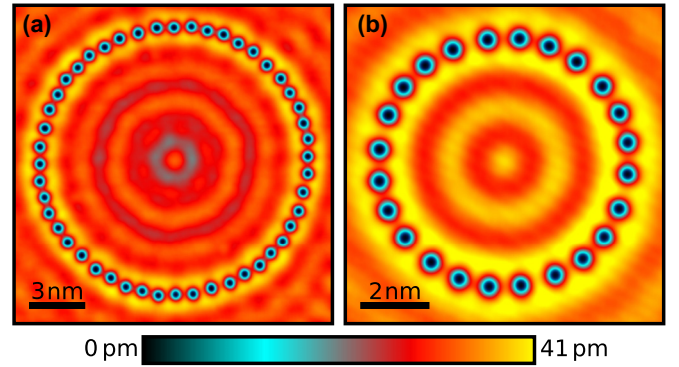


FIG. 1. (a) Constant current STM image (10 mV/10 pA) of the big 48-CO quantum corral, which has a radius of $R_{48,\text{large}} = 7.13$ nm. (b) STM image (50 mV/100 pA) of the small 24-CO quantum corral with a radius of $R_{24,\text{small}} = 3.57$ nm. Both corrals have an average intermolecular distance of 938 pm.

radius of $R_{48,\text{big}} = 7.13$ nm (48 CO molecules) and another with a radius of $R_{24,\text{small}} = 3.57$ nm (24 CO molecules). Both structures share an identical wall density with an average intermolecular distance of 938 pm. Detailed information on the construction plans of the two differently sized corrals is available in the Supplemental Material (SM2) [42]. STM topography images of these corrals are presented in Figs. 1(a) and 1(b).

III. LINE SHAPE ANALYSIS

To study the line shapes of the corral states, we performed scanning tunneling spectroscopy. However, performing stationary dI/dV measurements (fixing \bar{r}_{tip} and sweeping the bias voltage V_B) restricts analysis to the $l = 0$ states, drastically limiting the amount of analyzed states. The reason for this is that one cannot find a position \bar{r}_{tip} where a particular $l \neq 0$ state is energetically and spatially isolated. An example of this problem is shown in Fig. S4 of the Supplemental Material [42].

A complete description of the corral states includes their energetic and spatial characteristics. By using dI/dV line scans across the whole diameter of the corral (constant height measurements at a fixed sample bias) one can record the spatial behavior of the local density of states (LDOS) at a single energy eV_B , with e being the elementary charge. We performed line scans across both corrals over a bias range from -450 to 400 mV in increments of 5 mV.

Combining these dI/dV line scans results in Figs. 2(a) and 2(b), which represent spatially (horizontal axis) and energetically (vertical axis) resolved local density of states (color coding) map of the quantum corral.

Each dI/dV line scan [each horizontal line in Figs. 2(a) and 2(b)] consists of a combination of several different states that, due to an energetic overlap, contribute at different magnitudes to the local density of states. Previously, it has been suggested that the standing wave pattern observed within the structure using STM can be effectively described with a linear combination of corral states [14]. We extend this concept to

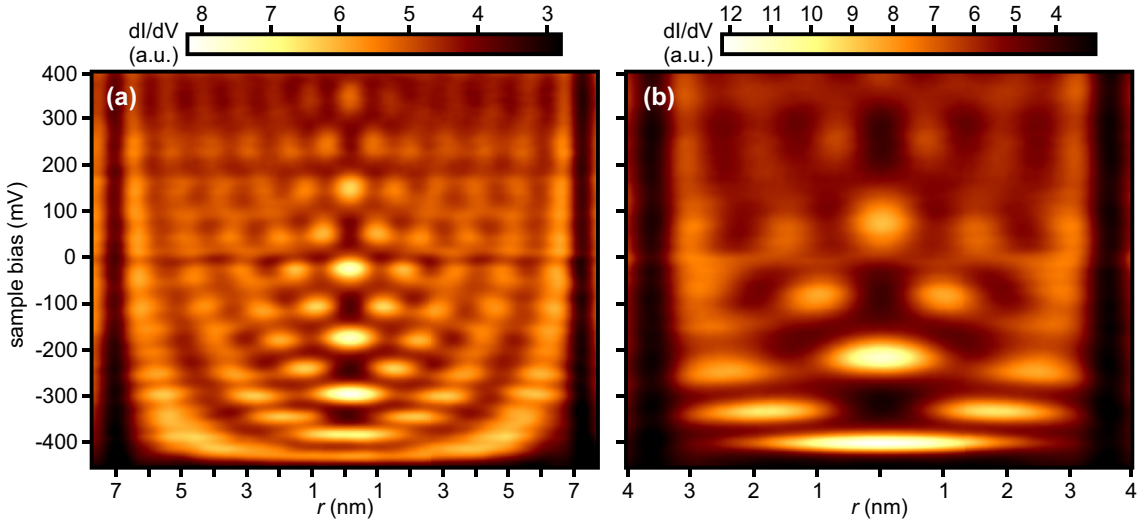


FIG. 2. Differential conductance (dI/dV) measurements are shown as a function of radial distance r from the center and sample bias for the (a) large 48-CO corral ($R_{48,\text{big}} = 7.13$ nm) and the (b) small 24-CO corral ($R_{24,\text{small}} = 3.57$ nm). In panels (a) and (b), respectively, the two outermost vertical, black stripes originate from the CO molecules (corral walls). The features that appear bright can be assigned to the corral states.

dI/dV line scans measured at different bias voltages:

$$\frac{dI}{dV}(r, eV_B) \propto \sum_{n,l} \alpha_{n,l}(eV_B) \times |\psi_{n,l}(r)|^2. \quad (1)$$

In this equation the prefactor $\alpha_{n,l}(eV_B)$ describes how much the probability density $|\psi_{n,l}(r)|^2$ contributes to the measured LDOS at a specific energy eV_B . Therefore, $\alpha_{n,l}(eV_B)$ is the energy distribution of the associated corral state. Additional details about applying Eq. (1) to determine $\alpha_{n,l}(eV_B)$ are given in the Supplemental Material (SM4) [42].

As an example a line scan obtained with a bias of -170 mV across the big corral and the corresponding fit using Eq. (1) is depicted in Fig. 3(a). The local density of states maps obtained from the right-hand side of Eq. (1) for the full bias range are presented in the Supplemental Material (SM5) [42], confirming that the corral states are well described by the linear combination of states with the weighting function $\alpha_{n,l}(eV_B)$.

Fitting Eq. (1) to the data allowed us to determine the energy distributions of several corral states, including $l \neq 0$ states. As a representative example, the energy distribution $\alpha_{4,1}$ ($n = 4$ and $l = 1$) of the big corral is shown in Fig. 3(b). All energy distributions $\alpha_{n,l}$ are given in the Supplemental Material (SM9) [42].

During dI/dV measurements there will always be three systematic broadening mechanisms which distort the shape of spectral peaks. First there is the temperature dependent widening of the Fermi-Dirac distribution [44], which we will call Fermi-broadening. A second source of spectral broadening is radio-frequency-broadening (RF-broadening) [45–48]. Both of these mechanisms cause a Gaussian shaped broadening of spectral features. Mathematically the combined broadening can be described by a convolution of two Gaussian terms: $G_{\text{Fermi,RF}} = G_{\text{Fermi}} * G_{\text{RF}}$. For the RF-broadening we estimate a FWHM (full width at half maximum) of $\Gamma_{\text{RF}} \approx 9$ meV [45,49] and for the Fermi-broadening at ≈ 5.7 K we

calculate $\Gamma_{\text{Fermi}} \approx 2$ meV [44]. In total these two mechanisms cause a Gaussian shaped broadening of spectroscopic peaks of $\Gamma_{\text{Fermi,RF}} \approx 9.2$ meV. The third mechanism of spectral broadening is modulation broadening which causes a broadening with the shape of a semicircle χ with a diameter of $2eV_{\text{mod}}$ [44,50].

To characterize the energetic behavior of the corral states we analyzed the energy distributions $\alpha_{n,l}$ in more detail. We first attempted to fit the spectral line shapes of the energy distributions by accounting for a Lorentzian line shape L with associated spectral width Γ_L , like it was proposed by Crommie *et al.* [14], as well as the broadening mechanisms $G_{\text{Fermi,RF}}$ and χ discussed above:

$$\alpha_{n,l} \propto L * G_{\text{Fermi,RF}} * \chi. \quad (2)$$

However, the fit resulted in rather poor agreement. This can be seen by the black dashed line for the energy distribution $\alpha_{4,1}$ in Fig. 3(b). We therefore incorporated a Gaussian line shape G_{wall} with associated width Γ_{wall} into the fitting function:

$$\alpha_{n,l} \propto L * G_{\text{wall}} * G_{\text{Fermi,RF}} * \chi. \quad (3)$$

In this equation the widths Γ_L and Γ_{wall} are parameters which account for the Lorentzian and Gaussian widths. The introduction of G_{wall} notably enhanced the fit quality, as evidenced by the improved agreement shown by the full blue line in Fig. 3(b). Interestingly, even with this refinement, accurately characterizing all $\alpha_{n,l}$ curves remained challenging. This is particularly true for energy distributions of states with the same main quantum number n and large angular momentum quantum number l since such states show a highly similar spatial behavior. As our approach involves extracting energy distributions from line scans, the fitting algorithm, employing Eq. (1), encounters complications in distinguishing between these closely related states. To characterize the accuracy of the energy distributions, a quality factor was introduced, as described in the Supplemental Material (SM6) [42]. We

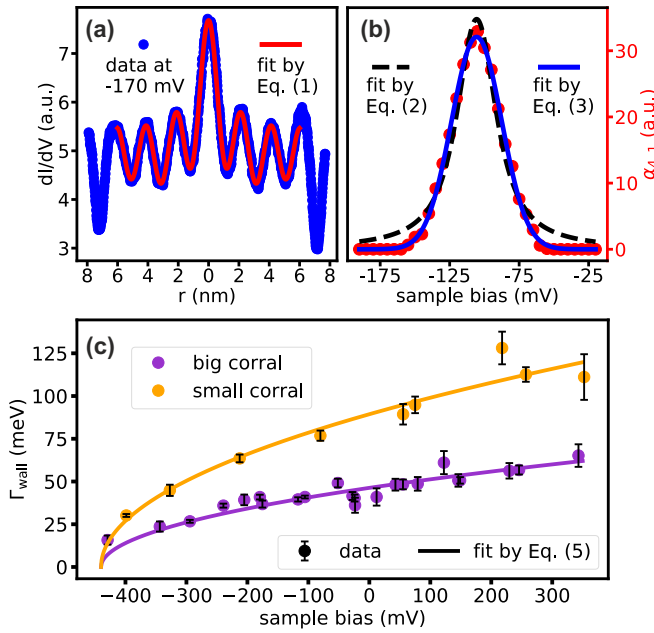


FIG. 3. (a) Blue: Measured dI/dV line scan at a sample bias of $V_B = -170$ meV across the big corral. Red: Fit of Eq. (1) to the measured curve. (b) Red dots: Energy distribution $\alpha_{4,1}$. The fit by Eq. (2) (Lorentzian and broadening terms), depicted as the black dashed line, exhibits a relatively poor agreement. The blue full line represents the fit by Eq. (3), which includes a Lorentzian (associated width Γ_L), a Gaussian (associated width Γ_{wall}), and broadening terms, provides an excellent agreement. (c) Purple markers: Γ_{wall} for the big corral ($R_{48,\text{big}} = 7.13$ nm). Orange markers: Γ_{wall} for the small corral ($R_{24,\text{small}} = 3.57$ nm). Full lines: Fit of the average path length model, described by Eq. (5), to the data points with the results: $x_{48,\text{big}} = (9.1 \pm 0.4)$ nm and $x_{24,\text{small}} = (4.7 \pm 0.3)$ nm.

constrain the remainder of the discussion to those energy distributions with a sufficient quality factor.

A representative example of a good fit is the $\alpha_{4,1}$ curve, depicted in Fig. 3(b). The following FWHM for the Lorentzian and Gaussian wall components were obtained: $\Gamma_L = (0 \text{ }_{(-)}^+ 2)$ meV and $\Gamma_{\text{wall}} = (41 \pm 1)$ meV. Throughout this article, the error bars represent two times the standard deviation obtained from fitting the data. These fitting parameters show, surprisingly, that the energy distribution $\alpha_{4,1}$ is described by a purely Gaussian peak shape. All energy distributions and the complementary fits with Eq. (3) are shown in SM9 [42].

We find the FWHM of the Gaussian component to be significantly larger than the Lorentzian component for all energy distributions. In fact, the Lorentzian component for most fits is negligible (equal to zero within uncertainty). The magnitudes (widths) of the Lorentzian and Gaussian wall components of the big and small corral are shown in the Supplemental Material (SM7) [42].

To further validate the results of our line scan fitting method, we compared the widths of the energy distributions and peak widths obtained from a static dI/dV measurement at the center of the big corral. This static measurement is only sensitive to the $l = 0$ states. This analysis is shown in the

Supplemental Material (SM8) [42] and yields the same values as the line scan fitting method.

By analyzing the properties of the energy distributions $\alpha_{n,l}(eV_B)$, we make several important conclusions. First, the energy distributions of corral states are poorly fit with a Lorentzian. This contrasts with existing literature, which suggests that the energy distributions have a Lorentzian shape [14]. Second, all distributions are fit well with a Gaussian curve (see SM7 and SM9 [42]). The width of the Gaussian curve, Γ_{wall} , shows a monotonic energy dependence [see Fig. 3(c)]. Finally, the overall magnitude of Γ_{wall} depends on the size of the corral.

IV. CHARACTERIZING THE SPECTRAL WIDTHS OF A CORRAL WITH A SINGLE PARAMETER

As discussed in the Introduction, there are several mechanisms that limit the lifetime of surface electrons: electron-phonon scattering, electron-electron scattering and electron-defect scattering. As presented in the previous section, the spectral widths show a monotonic energy dependence and a dependence on the corral size [see Fig. 3(c)] in agreement with previous theoretical calculations by Crampin *et al.* [51]. Similar to their results, we argue that the predominant lifetime limitation comes from the interaction of the surface electrons with the corral wall. This includes transmission (e.g., tunneling) through the potential barrier given by the CO-molecules and coupling to bulk states at the corral wall.

Due to the spatial homogeneity of electron-phonon scattering this decay mechanism is not sensitive to the size of quantum structures [21,24]. Additionally this mechanism results in a Lorentzian line shape. Therefore, it does not correlate with the observation that the spectral width is strongly dependent on the corral size and is better described by a Gaussian.

Calculations by Stilp *et al.* [41] showed that the total electron density for the small and big corral is the same (≈ 0.64 e⁻/nm²). Since electron-electron scattering scales with the total electron density [30,52–54] one can conclude that electron-electron scattering is also independent on the size of the quantum structure, even more it would also result in a Lorentzian line shape.

The negligible impact of electron-electron and electron-phonon scattering on the lifetime (inverse spectral width) of confined electron states in quantum structures has also been observed in vacancy islands on Ag(111) which had a similar size compared to our corrals [55].

Since both electron-electron and electron-phonon scattering cannot explain the observed Gaussian line shape and are insufficient to account for the size-dependent widths Γ_{wall} , we conclude that in our analyzed corrals the dominant lifetime limitation is mainly represented by the interaction of the surface electrons with the corral walls. This involves lateral transmission through the corral wall (e.g., tunneling) and scattering into bulk states (absorption). A detailed discussion about this will be presented in Sec. VI.

Crampin *et al.* [51] suggested a similar interaction mechanism to the one originally proposed by Heller *et al.* [31] to theoretically determine the lifetime of corral states including lossy scattering (that is, scattering including a loss term). In

literature, this loss term is often associated with coupling to bulk states (e.g., Refs. [31–33]). The model by Crampin *et al.* captures the trends we introduced earlier, demonstrating that smaller corrals host broader spectral peaks [see our data in Fig. 3(c)]. However, their theoretically derived energy dependence of the spectral peak widths shows a steeper slope than we observe in our experiments. Consequently, energetically lower lying peaks are underestimated in width, while those at higher energies are overestimated. This discrepancy most likely stems from the fact that the discussed theoretical calculations are not founded on CO-based quantum structures but rather on the “black-dot” limit (δ -peak-like scattering potentials with a purely absorbing channel), as introduced by Heller *et al.* for Fe-based corrals [31].

Here, we present a classical model to understand and characterize the dependence of the widths Γ_{wall} on energy. At its core, this classical description establishes a connection between Γ_{wall} and the average path length of a surface state electron. The model also yields a very good fit to our data.

The average path length x that an electron with a velocity of v_e can travel during its lifetime T_{life} is $x = v_e \times T_{\text{life}}$. Assuming that the velocity v_e can be deduced classically from the energy $E = eV_B + 440$ meV at which the electron is situated above the onset of the surface state band [56,57], the following equation is derived:

$$x = \sqrt{\frac{2(eV_B + 440 \text{ meV})}{m_e^*}} \times T_{\text{life}}. \quad (4)$$

Here m_e^* is the effective mass of surface state electrons on a Cu(111) surface which is 0.38 times the mass of a free electron [56,57]. By relating the spectral width to the lifetime via (the reduced) Planck’s constant, $T_{\text{life}} = \hbar/\Gamma$, the spectral width can be written as

$$\Gamma = \frac{\hbar \sqrt{\frac{2(eV_B + 440 \text{ meV})}{m_e^*}}}{x}. \quad (5)$$

The average path length x is then a parameter that is energy independent and can be determined for each corral by fitting Eq. (5) to the data points of Γ_{wall} from Fig. 3(c). The resulting fits yield values of $x_{48,\text{big}} = (9.1 \pm 0.4)$ nm and $x_{24,\text{small}} = (4.7 \pm 0.3)$ nm and are shown in Fig. 3(c).

The advantage of this model is threefold. First, it yields a very good agreement with the data and is therefore a good description of the energy dependence of Γ_{wall} . This again indicates that the dominant lifetime limitation of the corral states is the interaction of confined electrons with the corral wall. Second, we can compare the values of $x_{48,\text{big}}$ and $x_{24,\text{small}}$ and notice that they differ by a factor of 1.9 ± 0.3 which is the same factor of the difference in radius between the corrals ($R_{48,\text{large}}/R_{24,\text{small}} = 2$). This indicates, that for a fixed corral wall density the average path length scales with the radius of the corral. Third, it allows us to characterize a description of the lifetimes of the corral states (which are a function of energy) with a single parameter, the average path length x .

V. VARIATION OF THE WALL DENSITY

So far, we have presented data that shows that the lifetime of the corral states is directly related to the interaction of

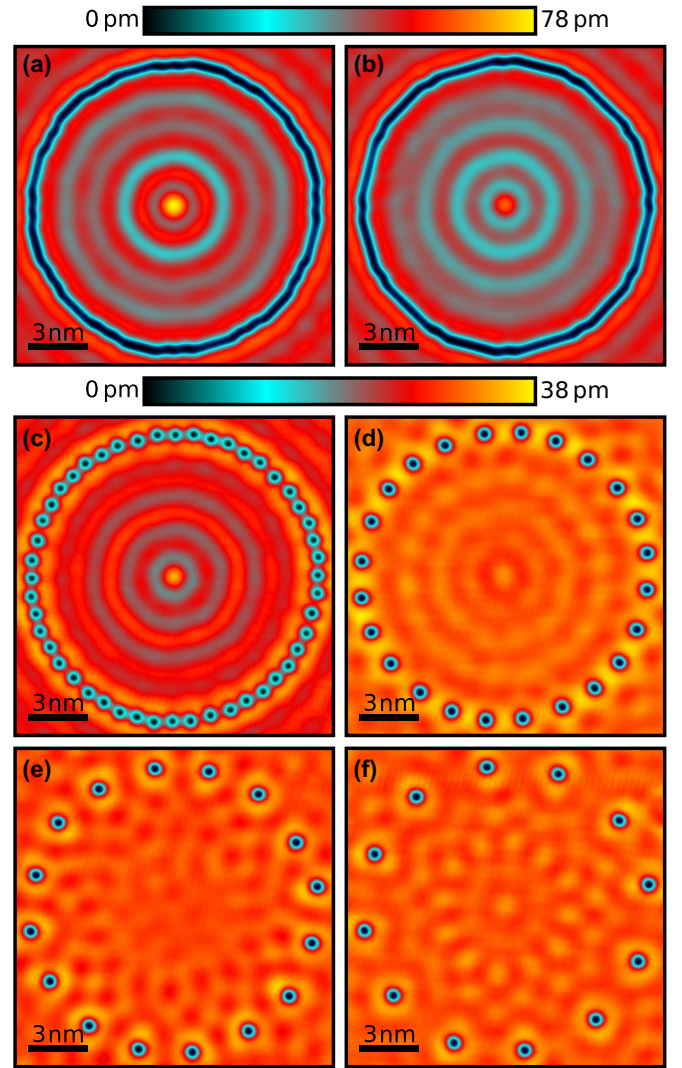


FIG. 4. Constant current STM images (-10 mV/100 pA) of the two 96-CO (a), (b), 48-CO (c), 24-CO (d), 16-CO (e), and 12-CO (f) quantum corrals. All depicted corrals, characterized by their wall densities, are constructed based on the CO adsorption sites of the 48-CO corral (c). Consequently, they share a common radius of 7.13 nm.

the surface state electrons with the corral walls. It is clear that lossy scattering is essential in describing the spectral widths, and therefore the lifetimes, of corral states. Recently scattering at the corral walls has been shown to couple corral states to bulk states of a superconducting substrate [17]. To better characterize the interaction with the walls, we determined the spectral widths of corral states for a range of wall densities. The wall density ρ_{wall} is defined as the number of CO molecules in the wall divided by the circumference of the corral.

The starting point for this investigation was the larger 48-CO corral, shown in Figs. 1(a) and 4(c). We built corrals of lower and higher wall densities, keeping the radius the same (7.13 nm), but incorporating 96, 24, 16, and 12 CO molecules in the walls, respectively. These corrals are shown in Fig. 4. Notably, in the case of the 96-CO corral, there are two possible configurations (96_1 and 96_2), that differ by

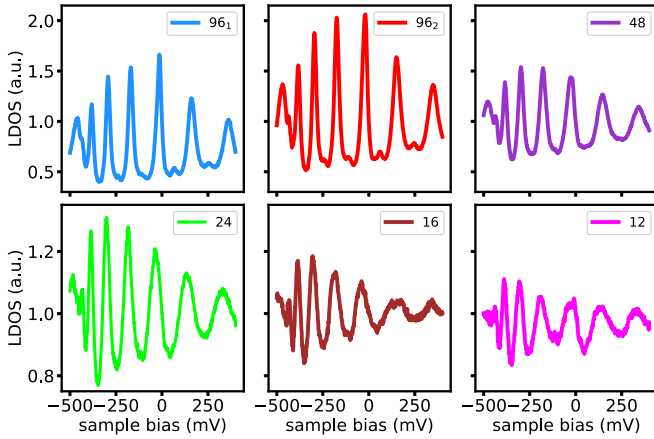


FIG. 5. Background removed differential conductance measurements [59] over the center of CO corrals with various wall densities and identical radius of 7.13 nm. Each spectrum is normalized at 0 mV sample bias. Each corral had the same radius but a varying amount of CO molecules in the wall. The number in the legend resembles the number of CO molecules in the corral wall. A large number of COs means a high wall density and vice versa.

one atomic adsorption site for a quarter of the CO molecules. The construction details, including the exact adsorption sites for all corrals, can be found in the Supplemental Material SM2 [42]. The average intermolecular distances (inverse wall density) of the 12-, 16-, 24-, 48-, 96₁-, and 96₂-CO-corrals are as follows: 3719 pm, 2792 pm, 1876 pm, 938 pm, and 477 pm (for both 96-CO-corrals). The 96-CO corrals have the maximum density, given that we require stable corral walls. In a previous study by Heinrich *et al.* [58], the stability of densely packed CO structures on a Cu(111) surface was investigated and it was revealed that structures with a higher density of CO undergo significant geometric changes in less than 1 min.

To characterize the effect of wall density on the lifetime (inverse spectral width) of corral states, we conducted static dI/dV measurements over the center of each corral. The background removed spectra [59] are shown in Fig. 5. Every spectrum in this plot is normalized at 0 mV sample bias.

The most apparent change when comparing the spectra are the widths of the spectral peaks, which decrease with increasing wall density. In both 96-CO spectra, small additional peaks emerge between the main $l = 0$ peaks. These smaller peaks can be attributed to $l \neq 0$ states. We believe this additional influence comes from the noninfinitesimal shape of the tip apex. For these measurements, we used a tip apex that ends in three metal atoms (verified with the COFI method [60]). The increased sensitivity for $l \neq 0$ states in dI/dV measurements over the center of a 96-CO corral with a non-infinitesimal tip apex is further amplified by the generally narrower widths of spectral peaks hosted in these denser corrals.

The resulting widths Γ_{wall} are depicted in Fig. 6. Again there is a strong energy dependence, as discussed previously. This data is also well described by Eq. (5), as shown by the solid lines in Fig. 6. Additionally, the Supplemental Material includes Fig. S20 (in SM10), depicting Γ_{wall} for the six corral types along with the corresponding fits using Eq. (5), each displayed as an individual plot [42].

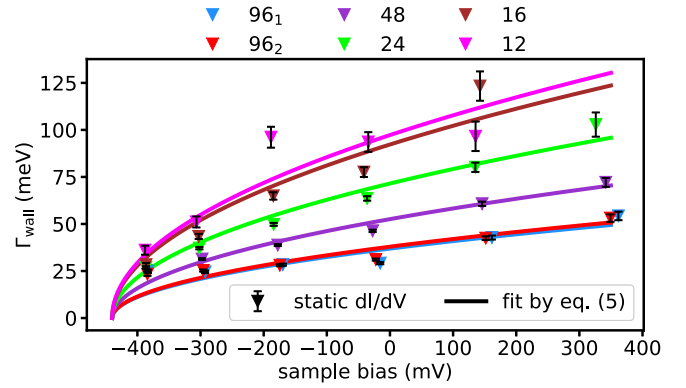


FIG. 6. Plot of Γ_{wall} for $l = 0$ states measured in the center of CO corrals with various wall densities and a common radius of 7.13 nm. The full lines are the fit of Eq. (5) to the datapoints to determine the average path length x of electrons in the quantum corral. The results: $x_{96_1} = (11.3 \pm 1.8)$ nm, $x_{96_2} = (11.5 \pm 2.0)$ nm, $x_{48} = (8.0 \pm 0.6)$ nm, $x_{24} = (6.1 \pm 0.3)$ nm, $x_{16} = (4.8 \pm 0.5)$ nm, and $x_{12} = (4.3 \pm 0.5)$ nm.

Figure 7 is a plot of the average path lengths of the surface electrons as a function of the wall density. As the CO molecules in the corral wall become more densely packed, the path length of surface state electrons increases. This is again in agreement with the theoretical consideration of Crampin *et al.* [51]. An empirical fit reveals that the average path length x exhibits a $\sqrt{\rho_{\text{wall}}}$ dependency (see full red line in Fig. 7).

VI. DISCUSSION

A. Relating spectral widths and corral wall density

As highlighted in Sec. IV, the primary factor limiting the lifetime of electrons in a quantum corral is their interaction with the wall. Generally, three mechanisms can occur when an electron interacts with the corral wall: reflection, absorption into bulk states and lateral transmission. The latter two represent lossy channels. An illustrative sketch of these three mechanisms is additionally given in the Supplemental

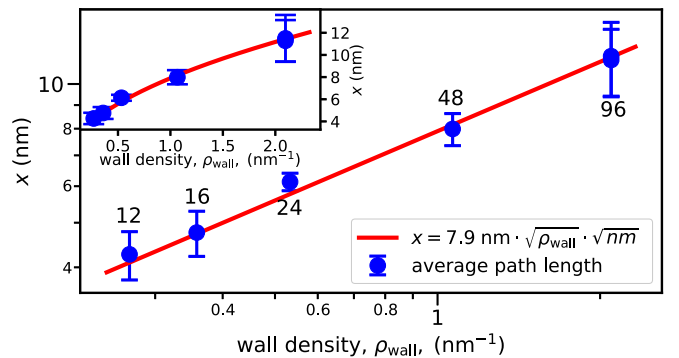


FIG. 7. Average path length x plotted with respect to the wall density ρ_{wall} in a logarithmic coordinates. Data points are depicted as blue markers. The numbers correspond to the number of CO-molecules in the corral wall. In the inset, a nonlogarithmic presentation of the main plot is provided. The solid red line represents the empirically found behavior.

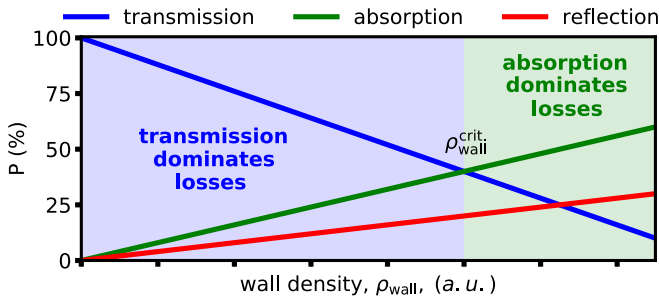


FIG. 8. Consideration about the three possibilities for electron-wall interaction: reflection, transmission (lossy) and absorption (lossy). The sum of all probabilities has to be equal to 100%. Our analysis revealed an increasing lifetime with a higher wall density, ρ_{wall} , meaning a positive slope for the reflection probability. At the critical wall density, $\rho_{\text{wall}}^{\text{crit}}$, the probability for transmission and absorption are equal. The linear representation of these probabilities in relation to ρ_{wall} is employed for illustrative purposes. The slopes of the presented curves are unknown, allowing for both possibilities: either the absorption line lies above the reflection line (shown in the plot), or vice versa (not shown). Nonetheless, the underlying conclusion remains consistent: as the wall density increases, the transmission probability decreases more rapidly than the absorption probability (scattering to bulk states) increases.

Material (SM11) [42]. If we consider these three possibilities, then the total probability of an electron interacting with the wall is expressed as $P_R + P_A + P_T = 100\%$. However, the respective probabilities (P_R for reflection, P_A for absorption, and P_T for transmission) change as a function of the wall density, ρ_{wall} .

For $\rho_{\text{wall}} = 0 \text{ nm}^{-1}$, the transmission probability P_T is 100% since absorption and reflection at the boundary are not possible. As ρ_{wall} increases P_T decreases and approaches 0 for $\rho_{\text{wall}} \rightarrow \infty$. Our experimental observations clearly show that corral lifetimes increase monotonically with wall density [see Figs. 3(c) and 6], meaning P_R monotonically increases with ρ_{wall} . If we accept that interaction of the surface state electrons with the corral walls includes a lossy channel to bulk states, then as ρ_{wall} increases, the number of lossy scatterers, and thus P_A , increase monotonically. These relations—the monotonic decrease of P_T from 100% with increasing ρ_{wall} , the monotonic increase of P_A and P_R , and the requirement that the sum of all probabilities adds up to 100%—are shown in Fig. 8. An interesting observation can be made: beyond a critical point ($\rho_{\text{wall}}^{\text{crit}}$), the dominant lossy channel changes from transmission to scattering to the bulk. This analysis shows that transmission is more sensitive to ρ_{wall} than absorption.

Several theoretical models propose different perspectives on the dominant lifetime limiting process in quantum corrals. Some point towards bulk coupling (absorption) as the primary process [31–33], while García-Calderón and Chaos-Cador [61], for instance, suggest that coherent processes, such as tunneling (transmission), play a more significant role. However, some theoretical considerations rely entirely on elastic mechanisms without coupling to the bulk [34,35]. Respecting all these theoretical considerations, we thus propose that corrals with a low wall density lie in the regime where transmission dominates, while for high wall density corrals,

absorption is the dominant lifetime limiting process. However, within this work we cannot determine the exact value of $\rho_{\text{wall}}^{\text{crit}}$.

B. Gaussian spectral shape

Up to now, literature uses Lorentzian-shaped curves to fit spectral peaks of quantum corrals (e.g., Refs. [14,55,62,63]). This implies an exponentially decaying survival probability of electrons within the corral. To satisfy this condition, electrons must exhibit a uniform decay probability for all times. However, our findings highlight that the primary mechanism limiting the lifetime of electrons in a quantum corral is their interaction with the wall. A single-particle approach, considering lossy interactions solely at the corral wall, is enough to yield a survival probability that does not exponentially decrease with time, as explicitly shown in (SM12) [42]. This challenges the exclusive description of spectral corral peaks with Lorentzian curves. We propose that a more complete theoretical picture will yield line shapes that are better described by a Gaussian rather than a Lorentzian function.

Gaussian-shaped spectral peaks in dI/dV measurements have been documented in literature, as observed in defects in salt layers [64] and quantum dots [65]. The Gaussian shapes were attributed to a strong coupling of a phonon mode with electrons. In the context of a corral, a plausible mode could be the coherent radial motion of CO molecules, also called breathing mode. The possibility of a direct, intermolecular interaction among individual CO molecules can be dismissed due to the substantial distance between them (e.g., 938 pm for the 48-corral). Nevertheless, it is a well-established fact that adsorbates can interact over extended distances through the surface state (e.g., Refs. [66–69]). Thus, the radially symmetric corral states could induce coherent motion of the COs. In the scenario of strong electron-phonon coupling, this coherent motion might offer an explanation for the Gaussian shape observed in the energy distributions presented in this paper. However, more comprehensive calculations are required that would go beyond the scope of this work.

The breathing mode could also directly affect of the energy of the corral states. The modulation of the corral radius induced by the coherent radial motion of the CO molecules would also influence the energetic position of the corral states. A reduction in radius elevates the states in energy, whereas an expansion in radius causes a downward shift. This variation in energy results in a widening of the measured spectral peak. To account for the experimentally determined spectral widths [see Figs. 3(c) and 6] via the effect of the breathing mode on corral states, radial amplitudes of 200 pm would be necessary. Details about this calculation are given in the Supplemental Material (SM13) [42]. Given that this value exceeds the radius of a copper atom (127 pm) and no shift in CO molecule positions occurred during the whole measurement period, we conclude that the energy shift of corral states due to the breathing mode does not represent a predominant mechanism for broadening.

Since the required amplitude is too large to fully account for the spectral width, we ask if the breathing mode could reasonably contribute to the measured spectral widths

assuming oscillation amplitudes as previously determined for single CO molecules. Viewing the breathing mode as a quantum mechanical oscillator (QMO) allows us to estimate its radial amplitude. The oscillation governs the corral's radius, and like any QMO, its ground state is characterized by a Gaussian curve. Consequently, the corral radius, modulated by the breathing mode, also adheres to a Gaussian curve. An approximation of the uncertainty in the position of a CO is about 33 pm [70]. Therefore, if the motion of the CO adsorbates is coherent, then it would, as a lowest estimate, contribute to a breathing mode induced Gaussian broadening of the energy distributions of approximately 4 meV at the Fermi energy and ≈ 8 meV for states 400 meV above the Fermi energy (for details see the Supplemental Material SM13 [42]).

In conclusion, we propose that the overall Gaussian shape of the energy distributions arises from (1) scattering of nonuniformly distributed scatterers, (2) strong coupling between electrons and a breathing mode, and (3) the effect of the breathing mode on the corral radii and the subsequent effect on the corral states.

VII. SUMMARY AND OUTLOOK

A. Summary

For the first part of our analysis we built two circular quantum corrals with different radii ($R_{48,\text{large}} = 7.13$ nm and $R_{24,\text{small}} = 3.57$ nm) but the same wall density on Cu(111). By comparing the measured local density of states with a linear combination of the probability density of the wave functions obtained from the hard wall model we determined the energy distributions, including those of $l \neq 0$ states. Analyzing these distributions revealed that the natural line shape is best described by a Gaussian function for all states. It also showed a correlation between the size of the corral and the spectral width, leading to the conclusion that the dominant lifetime limitation is governed by the interaction of electrons with the corral wall.

We thus proposed a classical model to relate the spectral widths of the corral states with the average path length of a surface state electron. This model describes the energy dependence of the spectral widths well.

To further characterize the electron-wall interaction, we constructed corrals with different wall densities. The widths of the spectral peaks decrease with increasing wall densities, clearly indicating longer corral state lifetimes for denser walls. This behavior prompted us to conclude that lateral transmission through the corral wall is more sensitive to the wall density than the coupling to bulk states at the corral boundary (CO molecules).

Finally, we discussed three possibilities to explain the observed Gaussian spectral shape. Currently, literature employs Lorentzian functions to fit spectral peaks of quantum corrals, assuming an exponential decay in electron survival. However, our findings suggest that the primary limitation to electron lifetimes in the corral arises from their interaction with the wall. This leads to a survival probability of the electrons in the corral that does not exponentially decrease with time, resulting in non-Lorentzian shaped spectral peaks. Another potential explanation, previously discussed in

literature for various sample systems, involves the coupling of electrons to specific phonon modes [64,65]. In the limit of strong electron-phonon coupling, Gaussian-shaped spectral peaks are observed. One plausible phonon mode in the case of quantum corrals is the breathing mode, representing a coherent movement of CO molecules in the wall. The coupling of electrons to this breathing mode can not only induce Gaussian-shaped peaks in spectra, but the breathing mode itself can influence the measured spectral line shape. While the estimated contribution of this variation in corral radius does not fully account for the measured widths, it may contribute to the overall Gaussian shape.

B. Outlook

Recent studies have shown that it is possible to prolong the lifetime of laterally confined field emission resonances by increasing either the vertical (z direction) or the lateral confinement dimensions (x - y plane) [71]. In the context of the work presented here, it was shown that the latter possibility is also applicable for adsorbate-based quantum corrals confining the Shockley surface state [see Fig. 3(c)]. In the following, three further methods for increasing the lifetime of quantum corral states are presented.

By adjusting the wall density within the range of approximately one order of magnitude, we observe a change in the average path length of an equivalent order of magnitude. If we were able to make a corral wall with adsorbates that allow nearest-neighbour occupation on each Cu sites, then we could hypothetically achieve a path length of ≈ 16 nm (by extrapolation of Fig. 7). While a denser corral wall is not possible, the radial thickness of the confinement can be increased by using a second or third row of CO molecules. It might be possible, with this approach, to reduce the lifetime limiting effects of tunneling (transmission) so drastically that the spectral widths are dominated by electron-electron, electron-phonon scattering and coupling to the bulk.

Another strategy for extending the lifetime of corral states involves employing different adsorbates for the corral wall. As discussed in Sec. VI B, a part of the Gaussian widths of the energy distributions could originate from the vibrational motion of the wall. By using adsorbates with a smaller vibrational amplitude than CO, this effect could be minimized (e.g., adsorbates which are bound more rigidly to the surface).

Lastly, in the pursuit of prolonging corral state lifetimes, it is important to consider the reduction of bulk coupling. As discussed in Sec. VI A, bulk coupling contributes significantly to the limitation of corral state lifetimes, especially at high wall densities. Exploring alternative adsorbates with diminished coupling to the bulk could mitigate this effect [54,72]. Additionally, the careful selection of the substrate offers a promising avenue for reducing bulk coupling. While such progress has already been demonstrated on a semiconductor substrate [6], the utilization of 2D layered materials could present a promising alternative for achieving similar outcomes.

ACKNOWLEDGMENTS

The authors thank A. Weindl and C. Setescaj for careful proofreading the manuscript and S. Tomsovic for fruitful discussions.

- [1] Y. F. Verolainen and A. Y. Nikolaich, Radiative lifetimes of excited states of atoms, *Sov. Phys. Usp.* **25**, 431 (1982).
- [2] M. A. Kastner, Artificial atoms, *Phys. Today* **46**(1), 24 (1993).
- [3] G. Schedelbeck, W. Wegscheider, M. Bichler, and G. Abstreiter, Coupled quantum dots fabricated by cleaved edge overgrowth: From artificial atoms to molecules, *Science* **278**, 1792 (1997).
- [4] J.-P. Jahn, M. Munsch, L. Béguin, A. V. Kuhlmann, M. Renggli, Y. Huo, F. Ding, R. Trotta, M. Reindl, O. G. Schmidt, A. Rastelli, P. Treutlein, and R. J. Warburton, An artificial Rb atom in a semiconductor with lifetime-limited linewidth, *Phys. Rev. B* **92**, 245439 (2015).
- [5] R. Pisoni, Z. Lei, P. Back, M. Eich, H. Overweg, Y. Lee, K. Watanabe, T. Taniguchi, T. Ihn, and K. Ensslin, Gate-tunable quantum dot in a high quality single layer MoS₂ van der Waals heterostructure, *Appl. Phys. Lett.* **112**, 123101 (2018).
- [6] E. Sierda, X. Huang, D. I. Badrtdinov, B. Kiraly, E. J. Knol, G. C. Groenenboom, M. I. Katsnelson, D. Wegner, and A. A. Khajetoorians, Quantum simulator to emulate lower-dimensional molecular structure, *Science* **380**, 1048 (2023).
- [7] S. Gao, S.-Y. Yin, Z.-X. Liu, Z.-D. Zhang, Z.-N. Tian, Q.-D. Chen, N.-K. Chen, and H.-B. Sun, Narrow-linewidth diamond single-photon sources prepared via femtosecond laser, *Appl. Phys. Lett.* **120**, 023104 (2022).
- [8] S. Pezzagna and J. Meijer, Quantum computer based on color centers in diamond, *Appl. Phys. Rev.* **8**, 011308 (2021).
- [9] T. D. Ladd, F. Jelezko, R. Laflamme, Y. Nakamura, C. Monroe, and J. L. O'Brien, Quantum computers, *Nature (London)* **464**, 45 (2010).
- [10] G. E. Cirlin, R. R. Reznik, I. V. Shtrom, A. I. Khrebtov, Y. B. Samsonenko, S. A. Kukushkin, T. Kasama, N. Akopian, and L. Leonardo, Hybrid GaAs/AlGaAs nanowire quantum dot system for single photon sources, *Semiconductors* **52**, 462 (2018).
- [11] M. Ruf, M. Ijspeert, S. van Dam, N. de Jong, H. van den Berg, G. Evers, and R. Hanson, Optically coherent nitrogen-vacancy centers in micrometer-thin etched diamond membranes, *Nano Lett.* **19**, 3987 (2019).
- [12] S. Ates, S. M. Ulrich, A. Ulhaq, S. Reitzenstein, A. Löffler, S. Höfling, A. Forchel, and P. Michler, Nonresonant dot-cavity coupling and its potential for resonant single-quantum-dot spectroscopy, *Nat. Photon.* **3**, 724 (2009).
- [13] P. C. Maurer, G. Kucsko, C. Latta, L. Jiang, N. Y. Yao, S. D. Bennett, F. Pastawski, D. Hunger, N. Chisholm, M. Markham, D. J. Twitchen, J. I. Cirac, and M. D. Lukin, Room-temperature quantum bit memory exceeding one second, *Science* **336**, 1283 (2012).
- [14] M. F. Crommie, C. P. Lutz, and D. M. Eigler, Confinement of electrons to quantum corrals on a metal surface, *Science* **262**, 218 (1993).
- [15] A. Zangwill, *Physics at Surfaces* (Cambridge University Press, Cambridge, UK, 1988).
- [16] W. Jolie, T.-C. Hung, L. Niggli, B. Verlhac, N. Hauptmann, D. Wegner, and A. A. Khajetoorians, Creating tunable quantum corrals on a Rashba surface alloy, *ACS Nano* **16**, 4876 (2022).
- [17] L. Schneider, K. T. Ton, I. Ioannidis, J. Neuhaus-Steinmetz, T. Posske, R. Wiesendanger, and J. Wiebe, Proximity superconductivity in atom-by-atom crafted quantum dots, *Nature (London)* **621**, 60 (2023).
- [18] M. Chen, Y.-P. Jiang, J. Peng, H. Zhang, C.-Z. Chang, X. Feng, Z. Fu, F. Zheng, P. Zhang, L. Wang, K. He, X.-C. Ma, and Q.-K. Xue, Selective trapping of hexagonally warped topological surface states in a triangular quantum corral, *Sci. Adv.* **5**, 1 (2019).
- [19] B. A. McDougall, T. Balasubramanian, and E. Jensen, Phonon contribution to quasiparticle lifetimes in Cu measured by angle-resolved photoemission, *Phys. Rev. B* **51**, 13891 (1995).
- [20] L. Bürgi, O. Jeandupeux, H. Brune, and K. Kern, Probing hot-electron dynamics at surfaces with a cold scanning tunneling microscope, *Phys. Rev. Lett.* **82**, 4516 (1999).
- [21] J. Kliewer, R. Berndt, E. V. Chulkov, V. M. Silkin, P. M. Echenique, and S. Crampin, Dimensionality effects in the lifetime of surface states, *Science* **288**, 1399 (2000).
- [22] P. M. Echenique, J. Oasma, M. Machado, V. M. Silkin, E. V. Chulkov, and J. M. Pitarke, Surface-state electron dynamics in noble metals, *Prog. Surf. Sci.* **67**, 271 (2001).
- [23] A. Fukui, H. Kasai, and A. Okiji, Many-body effects on the lifetime of Shockley states on metal surfaces, *Surf. Sci.* **493**, 671 (2001).
- [24] K. F. Braun and K. H. Rieder, Engineering electronic lifetimes in artificial atomic structures, *Phys. Rev. Lett.* **88**, 096801 (2002).
- [25] A. Eiguren, B. Hellsing, F. Reinert, G. Nicolay, E. V. Chulkov, V. M. Silkin, S. Hüfner, and P. M. Echenique, Role of bulk and surface phonons in the decay of metal surface states, *Phys. Rev. Lett.* **88**, 066805 (2002).
- [26] B. Hellsing, A. Eiguren, and E. V. Chulkov, Electron-phonon coupling at metal surfaces, *J. Phys.: Condens. Matter* **14**, 5959 (2002).
- [27] L. Vitali, P. Wahl, M. A. Schneider, K. Kern, V. M. Silkin, E. V. Chulkov, and P. M. Echenique, Inter- and intraband inelastic scattering of hot surface state electrons at the Ag(111) surface, *Surf. Sci.* **523**, L47 (2003).
- [28] M. G. Vergniory, J. M. Pitarke, and S. Crampin, Lifetimes of Shockley electrons and holes at Cu(111), *Phys. Rev. B* **72**, 193401 (2005).
- [29] E. V. Chulkov, A. G. Borisov, J. P. Gauyacq, D. Sánchez-Portal, V. M. Silkin, V. P. Zhukov, and P. M. Echenique, Electronic excitations in metals and at metal surfaces, *Chem. Rev.* **106**, 4160 (2006).
- [30] P. Hofmann, I. Y. Sklyadneva, E. D. L. Rienks, and E. V. Chulkov, Electron-phonon coupling at surfaces and interfaces, *New J. Phys.* **11**, 125005 (2009).
- [31] E. J. Heller, M. F. Crommie, C. P. Lutz, and D. M. Eigler, Scattering and absorption of surface electron waves in quantum corrals, *Nature (London)* **369**, 464 (1994).
- [32] S. Crampin, M. H. Boon, and J. E. Inglesfield, Influence of bulk states on laterally confined surface state electrons, *Phys. Rev. Lett.* **73**, 1015 (1994).
- [33] S. Crampin and O. R. Bryant, Fully three-dimensional scattering calculations of standing electron waves in quantum nanostructures: The importance of quasiparticle interactions, *Phys. Rev. B* **54**, R17367 (1996).
- [34] H. K. Harbury and W. Porod, Elastic scattering theory for electronic waves in quantum corrals, *Phys. Rev. B* **53**, 15455 (1996).
- [35] A. I. Rahachou and I. V. Zozoulenko, Elastic scattering of surface electron waves in quantum corrals: Importance of the shape of the adatom potential, *Phys. Rev. B* **70**, 233409 (2004).
- [36] J. Berwanger, F. Huber, F. Stilp, and F. J. Giessibl, Lateral manipulation of single iron adatoms by means of combined atomic force and scanning tunneling microscopy using CO-terminated tips, *Phys. Rev. B* **98**, 195409 (2018).

- [37] M. Ternes, C. P. Lutz, C. F. Hirjibehedin, F. J. Giessibl, and A. J. Heinrich, The force needed to move an atom on a surface, *Science* **319**, 1066 (2008).
- [38] M. R. Slot, T. S. Gardenier, P. H. Jacobse, G. C. P. van Miert, S. N. Kempkes, S. J. M. Zevenhuizen, C. M. Smith, D. Vanmaekelbergh, and I. Swart, Experimental realization and characterization of an electronic Lieb lattice, *Nat. Phys.* **13**, 672 (2017).
- [39] K. K. Gomes, W. Mar, W. Ko, F. Guinea, and H. C. Manoharan, Designer Dirac fermions and topological phases in molecular graphene, *Nature (London)* **483**, 306 (2012).
- [40] S. E. Freeney, S. T. P. Borman, J. W. Harteveld, and I. Swart, Coupling quantum corrals to form artificial molecules, *SciPost Physics* **9**, 085 (2020).
- [41] F. Stilp, A. Bereczuk, J. Berwanger, N. Mundigl, K. Richter, and F. J. Giessibl, Very weak bonds to artificial atoms formed by quantum corrals, *Science* **372**, 1196 (2021).
- [42] See Supplemental Material at <http://link.aps.org/supplemental/10.1103/PhysRevB.109.235422> for the experimental details (SM1), a description of the construction plans of the investigated corrals (SM2), the discussion of a stationary dI/dV measurement inside a quantum corral (SM3), a description how the line scan fitting was done (SM4), a consideration of the quality of the line scan fits (SM5), the mathematical description of the determination of the quality of an energy distribution (SM6), a comparison of the Gaussian and Lorentzian components of the energy distributions $\alpha_{n,l}(eV_B)$ (SM7), the comparison of peak widths obtained with line scan fitting and static dI/dV (SM8), all energy distributions with the complementary fits (SM9), Fig. 6 as individual plots (SM10), an illustration of the possible interaction mechanisms between an electron and the corral wall (SM11), the construction of a nonexponential survival probability for electrons in the corral based on our findings (SM12) and an estimate of the spectral broadening caused by a breathing mode induced corral radius variation (SM13). The Supplemental Material includes Refs. [43,59,70].
- [43] F. J. Giessibl, High-speed force sensor for force microscopy and profilometry utilizing a quartz tuning fork, *Appl. Phys. Lett.* **73**, 3956 (1998).
- [44] M. Ternes, Scanning tunneling spectroscopy at the single atom scale, Ph.D. thesis, Technische Universität Berlin, 2006.
- [45] A. Peronio, N. Okabayashi, F. Griesbeck, and F. Giessibl, Radio frequency filter for an enhanced resolution of inelastic electron tunneling spectroscopy in a combined scanning tunneling- and atomic force microscope, *Rev. Sci. Instrum.* **90**, 123104 (2019).
- [46] M. Assig, M. Etzkorn, A. Enders, W. Stiepany, C. R. Ast, and K. Kern, A 10 mK scanning tunneling microscope operating in ultra high vacuum and high magnetic fields, *Rev. Sci. Instrum.* **84**, 033903 (2013).
- [47] K. Bladh, D. Gunnarsson, E. Hürfeld, S. Devi, C. Kristoffersson, B. Smålander, S. Pehrson, T. Claeson, P. Delsing, and M. Taslakov, Comparison of cryogenic filters for use in single electronics experiments, *Rev. Sci. Instrum.* **74**, 1323 (2003).
- [48] H. le Sueur and P. Joyez, Microfabricated electromagnetic filters for millikelvin experiments, *Rev. Sci. Instrum.* **77**, 115102 (2006).
- [49] For the estimation of the RF-broadening in our setup we used the upper limit of the radio-frequency broadening obtained in another, similar LT and UHV microscope of our group. The value can be found in Ref. [45].
- [50] J. Klein, A. Léger, M. Belin, D. Défourneau, and M. J. Sangster, Inelastic-electron-tunneling spectroscopy of metal-insulator-metal junctions, *Phys. Rev. B* **7**, 2336 (1973).
- [51] S. Crampin, H. Jensen, J. Kröger, L. Limot, and R. Berndt, Resonator design for use in scanning tunneling spectroscopy studies of surface electron lifetimes, *Phys. Rev. B* **72**, 035443 (2005).
- [52] J. J. Quinn and R. A. Ferrell, Electron self-energy approach to correlation in a degenerate electron gas, *Phys. Rev.* **112**, 812 (1958).
- [53] P. M. Echenique, R. Berndt, E. V. Chulkov, T. Fauster, A. Goldmann, and U. Höfer, Decay of electronic excitations at metal surfaces, *Surf. Sci. Rep.* **52**, 219 (2004).
- [54] S. Heers, P. Mavropoulos, S. Lounis, R. Zeller, and S. Blügel, Lifetime reduction of surface states at Cu, Ag, and Au(111) caused by impurity scattering, *Phys. Rev. B* **86**, 125444 (2012).
- [55] H. Jensen, J. Kröger, R. Berndt, and S. Crampin, Electron dynamics in vacancy islands: Scanning tunneling spectroscopy on Ag(111), *Phys. Rev. B* **71**, 155417 (2005).
- [56] S. D. Kevan, Evidence for a new broadening mechanism in angle-resolved photoemission from Cu(111), *Phys. Rev. Lett.* **50**, 526 (1983).
- [57] M. F. Crommie, C. P. Lutz, and D. M. Eigler, Imaging standing waves in a two-dimensional electron gas, *Nature (London)* **363**, 524 (1993).
- [58] A. J. Heinrich, C. P. Lutz, J. A. Gupta, and D. M. Eigler, Molecule cascades, *Science* **298**, 1381 (2002).
- [59] P. Wahl, L. Diekhöner, M. A. Schneider, and K. Kern, Background removal in scanning tunneling spectroscopy of single atoms and molecules on metal surfaces, *Rev. Sci. Instrum.* **79**, 043104 (2008).
- [60] J. Welker and F. J. Giessibl, Revealing the angular symmetry of chemical bonds by atomic force microscopy, *Science* **336**, 444 (2012).
- [61] G. García-Calderón and L. Chaos-Cador, Theory of coherent and incoherent processes in quantum corrals, *Phys. Rev. B* **73**, 195405 (2006).
- [62] S. Crampin, Scanning tunneling spectroscopy of surfaces where surface states dominate, *J. Electron Spectrosc. Relat. Phenom.* **109**, 51 (2000).
- [63] J. Kliewer, R. Berndt, and S. Crampin, Scanning tunnelling spectroscopy of electron resonators, *New J. Phys.* **3**, 22 (2001).
- [64] J. Repp, G. Meyer, S. Paavilainen, F. E. Olsson, and M. Persson, Scanning tunneling spectroscopy of Cl vacancies in NaCl films: Strong electron-phonon coupling in double-barrier tunneling junctions, *Phys. Rev. Lett.* **95**, 225503 (2005).
- [65] L. Jdira, K. Overgaard, R. Stiuflu, B. Grandidier, C. Delerue, S. Speller, and D. Vanmaekelbergh, Linewidth of resonances in scanning tunneling spectroscopy, *Phys. Rev. B* **77**, 205308 (2008).
- [66] K. H. Lau and W. Kohn, Indirect long-range oscillatory interaction between adsorbed atoms, *Surf. Sci.* **75**, 69 (1978).
- [67] B. Gumhalter and W. Brenig, Indirect adsorbate-adsorbate interactions mediated by quasi-one-dimensional surface electronic states, *Prog. Surf. Sci.* **48**, 39 (1995).
- [68] P. Hyltdgaard and M. Persson, Long-ranged adsorbate-adsorbate interactions mediated by a surface-state band, *J. Phys.: Condens. Matter* **12**, L13 (2000).

- [69] P. Hyldgaard and T. L. Einstein, Surface-state mediated three-adsorbate interaction: Exact and numerical results and simple asymptotic expression, *Appl. Surf. Sci.* **212-213**, 856 (2003).
- [70] N. Okabayashi, A. Peronio, M. Paulsson, T. Arai, and F. J. Giessibl, Vibrations of a molecule in an external force field, *Proc. Natl. Acad. Sci. USA* **115**, 4571 (2018).
- [71] R. Rejali, L. Farinacci, D. Coffey, R. Broekhoven, J. Gobeil, Y. M. Blanter, and S. Otte, Confined vacuum resonances as artificial atoms with tunable lifetime, *ACS Nano* **16**, 11251 (2022).
- [72] J. Fernández, M. Moro-Lagares, D. Serrate, and A. A. Aligia, Manipulation of the surface density of states of Ag(111) by means of resonators: Experiment and theory, *Phys. Rev. B* **94**, 075408 (2016).